



## Endosomal pH modulation by peptide-gold nanoparticle hybrids enables potent anti-inflammatory activity in phagocytic immune cells



Hong Yang<sup>a,b,\*</sup>, Lisa Kozicky<sup>a</sup>, Aabida Saferali<sup>a</sup>, Shan-Yu Fung<sup>a</sup>, Nicole Afacan<sup>c</sup>, Bing Cai<sup>a</sup>, Reza Falsafi<sup>c</sup>, Erin Gill<sup>c</sup>, Mingyao Liu<sup>d</sup>, Tobias R. Kollmann<sup>a</sup>, R.E.W. Hancock<sup>c</sup>, Laura M. Sly<sup>a</sup>, Stuart E. Turvey<sup>a,\*\*</sup>

<sup>a</sup> BC Children's Hospital and Child & Family Research Institute, Department of Pediatrics, Faculty of Medicine, University of British Columbia, Vancouver, BC V5Z 4H4, Canada

<sup>b</sup> Department of Respiratory Medicine, Shanghai First People's Hospital, Shanghai Jiaotong University School of Medicine, Shanghai 201620, China

<sup>c</sup> Department of Microbiology and Immunology, Centre for Microbial Diseases and Immunity Research, University of British Columbia, Vancouver, BC V6T 1Z4, Canada

<sup>d</sup> Latner Thoracic Surgery Research Laboratories, Toronto General Research Institute, University Health Network, Department of Surgery, Faculty of Medicine, University of Toronto, Toronto, Ontario, M5G 1L7, Canada

### ARTICLE INFO

#### Article history:

Received 6 August 2016

Received in revised form

22 September 2016

Accepted 26 September 2016

Available online 3 October 2016

#### Keywords:

Nanoparticle

Peptide-conjugation

Anti-inflammatory therapeutics

Toll-like receptor signaling

Immune modulation

Inflammatory bowel disease

### ABSTRACT

Toll-like receptor (TLR) signaling plays a central role in the pathophysiology of many acute and chronic human inflammatory diseases, and pharmacological regulation of TLR responses is anticipated to be beneficial in many inflammatory conditions. Currently there are no specific TLR inhibitors in clinical use. To overcome this challenge, we have developed a nano-based TLR inhibitor (peptide-gold nanoparticle hybrids) that inhibits a broad spectrum of TLR responses. Through mechanistic studies, we established that specific peptide decorated-gold nanoparticles that display high cellular uptake in phagocytic immune cells modulate endosomal pH, leading to significant attenuation of signaling through multiple TLRs. Using a global transcriptomic approach, we defined the broad anti-inflammatory activity of the nanoparticle in human peripheral blood mononuclear cells. *In vivo* studies confirmed the beneficial immunomodulatory activity since treatment with the nanoparticle significantly reduced weight loss, improved the disease activity index, and ameliorated colonic inflammation in a murine model of intestinal inflammation. This work enhances our fundamental understanding of the role of peptide coatings on the nanoparticle surface in regulating innate immune signaling, and identifies specific peptide decorated nanoparticles that may represent a novel class of anti-inflammatory therapeutics for human inflammatory diseases.

© 2016 Elsevier Ltd. All rights reserved.

The innate immune system and Toll-like receptor (TLR) signaling play a vital role in host defense against infections. TLRs can recognize and respond to diverse microbial epitopes—pathogen-associated molecular patterns (PAMPs)—enabling the innate

\* Corresponding author. BC Children's Hospital and Child & Family Research Institute, Department of Pediatrics, Faculty of Medicine, University of British Columbia, Vancouver, BC V5Z 4H4, Canada. Department of Respiratory Medicine, Shanghai First People's Hospital, Shanghai Jiaotong University School of Medicine, Shanghai 201620, China.

\*\* Corresponding author. BC Children's Hospital and Child & Family Research Institute, Department of Pediatrics, Faculty of Medicine, University of British Columbia, Vancouver, BC V5Z 4H4, Canada.

E-mail addresses: [hongyang36@gmail.com](mailto:hongyang36@gmail.com) (H. Yang), [sturvey@cw.bc.ca](mailto:sturvey@cw.bc.ca) (S.E. Turvey).

<http://dx.doi.org/10.1016/j.biomaterials.2016.09.032>

0142-9612/© 2016 Elsevier Ltd. All rights reserved.

immune system to identify pathogens and to induce an appropriate cascade of protective effector responses [1]. However, like a 'double-edged sword', vigorous TLR responses can be harmful, contributing to pathology in many acute and chronic human inflammatory diseases, such as sepsis, cystic fibrosis, asthma, a variety of autoimmune diseases and cancer [2,3]. Therefore, tight regulation of TLR signaling is anticipated to be essential in treating many human inflammatory conditions [3,4].

Pharmacological inhibitors and antagonists that down-regulate excessive TLR signaling are predicted to be effective in controlling damaging inflammation and to be beneficial in treating many autoimmune diseases [5]. Unfortunately, there are only a few TLR inhibitors/antagonists that have been advanced to clinical trials, and so far there have been no TLR inhibitors approved for clinical

use. One of the most advanced TLR antagonists was Eritoran, a lipopolysaccharide (LPS)-mimicking TLR4 antagonist [6]. However, in a phase III clinical trial, Eritoran did not show significant therapeutic benefit in treating severe sepsis, perhaps due to the immune complexity of sepsis or because multiple pattern recognition receptor (PRR) pathways are often involved in responding to any infection. Nevertheless, this failure of a clinical trial involving a specific TLR4 inhibitor informs us that blocking one signaling pathway may not be sufficient to ameliorate established disease. Thus, there is a great need to develop a new generation of TLR inhibitors that are potent and able to target to multiple TLR signaling pathways.

Accumulating evidence has shown that TLR signaling is tightly associated with endocytosis [7], and that endosomes are an essential site for signal transduction by multiple TLRs [8]. In the case of TLR4 pathway, this signaling cascade consists of two arms: MyD88-dependent and MyD88-independent (or TRIF-dependent) signaling. The MyD88-independent pathway originates from the endosome, and it signals through internalized TLR4 ligand LPS that binds with TLR4 in the endosome. It has been established that the endosomal trafficking of endocytosed LPS is associated with termination of the MyD88-dependent signal; inhibition of endocytosis thus enhances the MyD88-dependent signaling [9]. Therefore, selectively manipulating endosomal receptor signaling could provide a novel way to broadly regulate TLR signaling.

Bioactive nano-devices preferentially targeting endosomes may provide a new strategy to modulate TLR signaling and treat human inflammatory diseases. Rapid advances in nano-science and technology have contributed to the creation of diverse materials with thoughtfully-designed surface chemistry and functional properties. For example, using rational design principles to tailor functionality, nanoparticles can preferentially target phagocytic innate immune cells [10], making them a compelling new generation of therapeutic agents to modulate immune responses for various diseases [11–16]. Additionally, nanoparticles can optimize therapeutic outcomes by improving *in vivo* biodistribution and sustaining the release of drugs [17–19].

Our research objective is to develop new potent nano-inhibitors of TLR signaling with beneficial anti-inflammatory activity for treating human inflammatory diseases. To achieve this goal, we constructed a library of physiologically stable peptide-gold nanoparticle hybrids with tunable surface chemistry (via different peptide ligands), to serve as a “nano-drug” discovery platform [20,21]. Applying a high throughput screening approach, we discovered a lead nanoparticle that exhibited broad inhibitory activity on multiple TLRs. In the current study, we made significant advances in understanding the novel mechanism(s) of action of the lead nanoparticle and establishing their therapeutic activity *in vivo*. In addition, we used unbiased global transcriptome analysis to define the spectrum of the anti-inflammatory activity of the lead nanoparticle in primary human immune cells. This research provides mechanistic understanding of the role played by the peptides conjugated on the nanoparticle surface in regulating TLR signaling, and identifies specific nanoparticle hybrids that represent a novel class of anti-inflammatory therapeutics for human inflammatory diseases.

## 1. Results

**Global transcriptomic analysis to define the bioactivity of the peptide-gold nanoparticle (GNP) hybrids in primary human immune cells.** In our previous studies we constructed a novel nanoparticle hybrid system. The nano-hybrid was made of a gold nanoparticle core and a peptide coating (Fig. 1a). The peptide coatings allow programming of the nanoparticle surface chemistry,

to enhance the physiological stability of the nanoparticles and enable the immune modulatory activity [20,21]. Through screening, we identified one lead product (designated P12) that exhibited potent anti-inflammatory activity [22]. P12 was coated with a peptide containing two phenylalanine (F) residues in the sequence (CLPFFD); interestingly, P13 (the sequence of the decorated peptide: CLPAAD), which only differs from P12 by a change of phenylalanine to alanine (A) in the peptide sequence, had no inhibitory activity and served as our control.

To globally assess the anti-inflammatory activity of P12, the high throughput cDNA sequencing method RNA-Seq was used to analyze the global effects of the P12 nanoparticles, compared with the control P13 nanoparticles, on the LPS-induced transcriptome of human peripheral blood mononuclear cells (PBMC,  $n = 4–5$  healthy donors). Principal component analysis (PCA) of differentially expressed genes (Fig. 1b) and hierarchical clustering analysis (Fig. S1), demonstrated that samples in each treatment group clustered together, with a clear separation between unstimulated and LPS stimulated groups. P12 treatment globally attenuated LPS-mediated gene expression shifting this group closer to the untreated controls, while P13 had no significant effect and the P13 treatment group was indistinguishable from that of LPS alone.

A total of 880 genes (approximately 3.5% of the transcriptome) changed expression by more than two fold following LPS stimulation. Of these 880 LPS-responsive genes, 572 genes were up-regulated and 308 were down-regulated (Fig. 1c). P12 treatment suppressed the expression of 233 of the genes up-regulated by LPS stimulation and 29 of the genes down-regulated by LPS. Overall, about 40% of genes that were up-regulated by LPS in human PBMC were suppressed by P12. As expected, the control nanoparticle P13 had almost no effect on the LPS-responsive genes, and only 3 LPS up-regulated genes were suppressed by P13 (Fig. 1c). The potent effect of P12 on normalizing gene expression profiles of human PBMC following LPS stimulation was visualized using a gene expression heat map (Fig. 1d) in which the top 33 differentially expressed genes (cut-off  $p$ -value is  $2.6 \times 10^{-15}$ ) were displayed with the P12 treatment group exhibiting a similar gene expression pattern to the unstimulated controls, while P13 treatment had little impact on LPS-stimulated gene expression. The impact of P12 on all differentially expressed genes is shown in the Supporting Information (Fig. S2).

To better classify the biological processes modulated by P12 in LPS-treated PBMC, we performed pathway and Gene Ontology (GO) analysis (with Bonferroni corrected  $p$ -value of 0.05) using functional annotation from the DAVID Bioinformatics Resources and Sigora. We found that the P12-modulated LPS responsive transcripts were genes largely associated with immune system processes, response to stimulus, and biological regulation (Table S1). From Innate DB and Sigora pathway analysis, we identified a number of key inflammatory pathways that were inhibited by P12, but not P13 (Table 1); including the Toll like receptor (TLR), protein kinase R (PKR), interferon, tumor necrosis factor- $\alpha$  (TNF), chemokine and Janus kinase and Signal Transducer and Activator of Transcription (JAK-STAT) signaling pathways. These data confirmed the broad immunomodulatory activity of P12 and also supported the potential for clinical translation since each of these signaling pathways have been identified to be strongly associated with inflammatory responses central to the pathogenesis of many inflammatory diseases (e.g., inflammatory bowel disease) [23,24].

**P12 inhibits pro-inflammatory cytokine production by primary immune cells.** The anti-inflammatory activity of P12 in primary human immune cells was further evaluated by profiling the production of a broad spectrum of cytokines using a multiplexed cytokine assay. We found that P12 inhibited the production of multiple chemokines and cytokines that are normally secreted

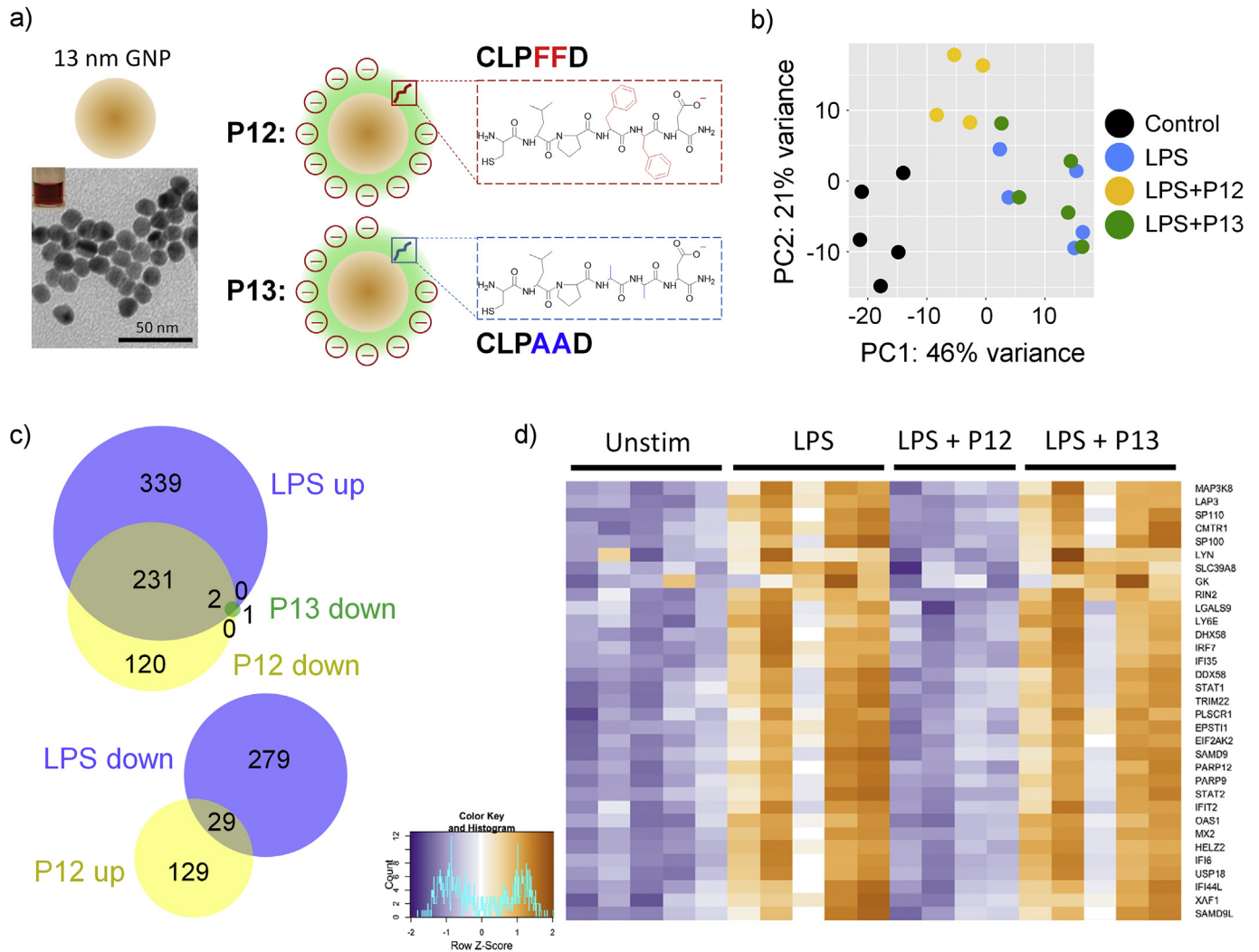


**Fig. 1.** Impact of anti-inflammatory nanoparticle P12 treatment on RNA-Seq transcriptome analysis of LPS-stimulated human PBMC. (a) Novel peptide-decorated nanoparticle hybrids with different surface chemistry (P12 vs. P13). (b) PCA plot. (c) Venn diagrams. (d) Differential expression profiles of top 33 genes ( $p < 2.6 \times 10^{-15}$  and fold change  $> 1.5$ ).

following LPS stimulation, including MCP-1, MCP-3, IP-10, IL-12p40, IL-23 and interferons (Fig. 2a). Interestingly, P12 also significantly increased secretion of the anti-inflammatory cytokine IL-1RA. Again, the control nanoparticle (P13) had almost no effect on LPS-stimulated cytokine production, confirming that the anti-inflammatory activity of P12 was peptide-sequence specific. Selected cytokines (MCP-1, IL-12p40 and IL-1RA) were independently validated using ELISA (Fig. 2b–d). Together, these results confirmed the promising anti-inflammatory activity of P12 through inhibition of a broad spectrum of pro-inflammatory cytokine production.

**Peptide-GNP hybrids preferentially target phagocytic immune cells in the PBMC population.** From both global transcriptomic analysis and cytokine profiling, the compelling anti-inflammatory activity of P12 was established in LPS-stimulated human PBMC. Next, we sought to determine which types of cells within the mixed PBMC population were targeted by the nanoparticles. To achieve this, fluorescent anti-inflammatory nanoparticles were developed by conjugating Cy5-labeled polyethylene glycol (PEG) chains (with Cy5-PEG to peptide molar ratio of 1:200) to P12 and P13 (Fig. 3a). Importantly, this fluorescent version of P12 retained the capacity to inhibit both the NF- $\kappa$ B and IRF pathways

**Table 1**

List of the most highly represented biological pathways of P12 regulated genes in LPS stimulated PBMC.

Pathway names	Bonferroni corrected P value
PKR signaling	$<10^{-300}$
Interferon signaling	$1.03 \times 10^{-271}$
TLR signaling	$3.27 \times 10^{-64}$
Chemokine signaling	$9.87 \times 10^{-29}$
JAK-STAT signaling pathway	$1.75 \times 10^{-22}$
TNF signaling	$1.27 \times 10^{-10}$

associated with TLR4 signaling, albeit with slightly reduced potency; while the fluorescent version of P13 remained inactive (Fig. 3b). Using these fluorescent nanoparticles together with multi-parameter flow cytometric analysis (Fig. 3c), we found that the majority of nanoparticles were taken up by phagocytic cells, particularly monocytes, myeloid dendritic cells (mDCs) and plasmacytoid DCs (pDCs) (Fig. 3d). Interestingly, there was no significant difference between P12 and P13 in the distribution of these nanoparticles among different cell types (Fig. 3e), indicating that both the anti-inflammatory and inactive nanoparticles targeted the

same phagocytic cell populations in PBMC.

### The peptides conjugated on the nanoparticle surface program cellular uptake and modulate anti-inflammatory activity.

To elucidate the mechanisms of action by which P12 reduces the inflammatory responses triggered through TLR4 in phagocytic immune cells, we chose THP-1 cells (a human monocytic cell line) and THP-1-derived macrophages as a human phagocytic immune cell model. We found that P12 and P13 were not toxic to these cells (Fig. S3). The cellular uptake of the nanoparticle hybrids into THP-1 monocyte and THP-1-derived macrophages was quantified by measuring the optical absorbance (at 526 nm) of the cell lysates in comparison to a standard curve of the optical absorbance of known concentrations of nanoparticles in the lysis buffer. As shown in Fig. 4a, the uptake of P12 in the THP-1 monocytes was 0.44 pmol/10<sup>5</sup> cells, whereas the uptake of P13 was significantly lower at <0.03 pmol/10<sup>5</sup> cells ( $P < 0.001$ ). For THP-1-derived macrophages, which have a higher phagocytic activity, the uptake of P12 and P13 were again significantly different at 1.2 and 0.3 pmol/10<sup>5</sup> cells, respectively ( $P < 0.001$ ). This trend was also reflected from the UV–Vis spectra measurement of the extracted internalized nanoparticles (Fig. 4b). Microscopic inspection of the cells confirmed the higher uptake of P12 compared with P13 (Fig. 4c and d). The significantly higher uptake of P12 compared to P13 in both monocytes and macrophages was likely due to the presence of phenylalanine (F) on the P12 nanoparticle surface, as demonstrated in our earlier studies that the presence of amino acids with aromatic ring structure on the nanoparticle surfaces enhances the cellular uptake of the nanoparticles [20,21].

To establish the relationship between the nanoparticle cellular uptake and inhibitory activity of the nanoparticles in TLR4 signaling, we further measured the uptake of a small library of the

peptide-GNP hybrids into THP-1 cell derived macrophages and their corresponding inhibitory activities on NF- $\kappa$ B and IRF activation (Fig. 5). These hybrids were coated with a variety of peptides that differ in only two amino acids in the peptide sequence (Fig. 5a). We plotted the inhibitory activity of each nanoparticle hybrid as a function of the cellular uptake (Fig. 5b and c). We found that the inhibitory activities of the nanoparticles on both NF- $\kappa$ B and IRF activation of TLR4 signaling correlate well with their cellular uptake (the correlation coefficients are 0.82 and 0.78 for NF- $\kappa$ B and IRF pathway, respectively). The higher the cellular uptake, the stronger the inhibition on both NF- $\kappa$ B and IRF activation.

**Nanoparticles with higher cellular uptake modulate endosomal pH.** Endosomal pH is recognized to play an important role for endosomal TLR signaling [25–27]. P12 and P13 were confirmed to localize in endosomal and lysosomal vesicles (Fig. S4). Based on the high uptake of P12 into the endosomal compartments of phagocytic cells and the negative charge on the nanoparticle surface conferred by the terminal aspartate (D) [21,22], we hypothesized that P12 modulates endosomal pH, thus contributing to the observed inhibition of TLR4 signaling. To test this hypothesis, the impact of P12 on endosomal pH was analyzed by comparison with the classic endosomal pH modulators, bafilomycin (BAF, an inhibitor of vacuolar H<sup>+</sup> ATPase) and chloroquine (CQ, a lysosomotropic agent that prevents endosomal acidification). Changes in endosomal pH were probed with fluorescein- and pHrodo red-labeled dextran (10,000 MW) [28]. Both probes are pH sensitive since fluorescein has a strong fluorescence emission in a neutral environment (pH 6–7.2), while the emission of pHrodo red gradually decreases as the pH rises (pH 4–8). Thus, the fluorescence intensity ratio of fluorescein/pHrodo red can be used to indicate pH change in the endosomal compartments, with higher values indicating

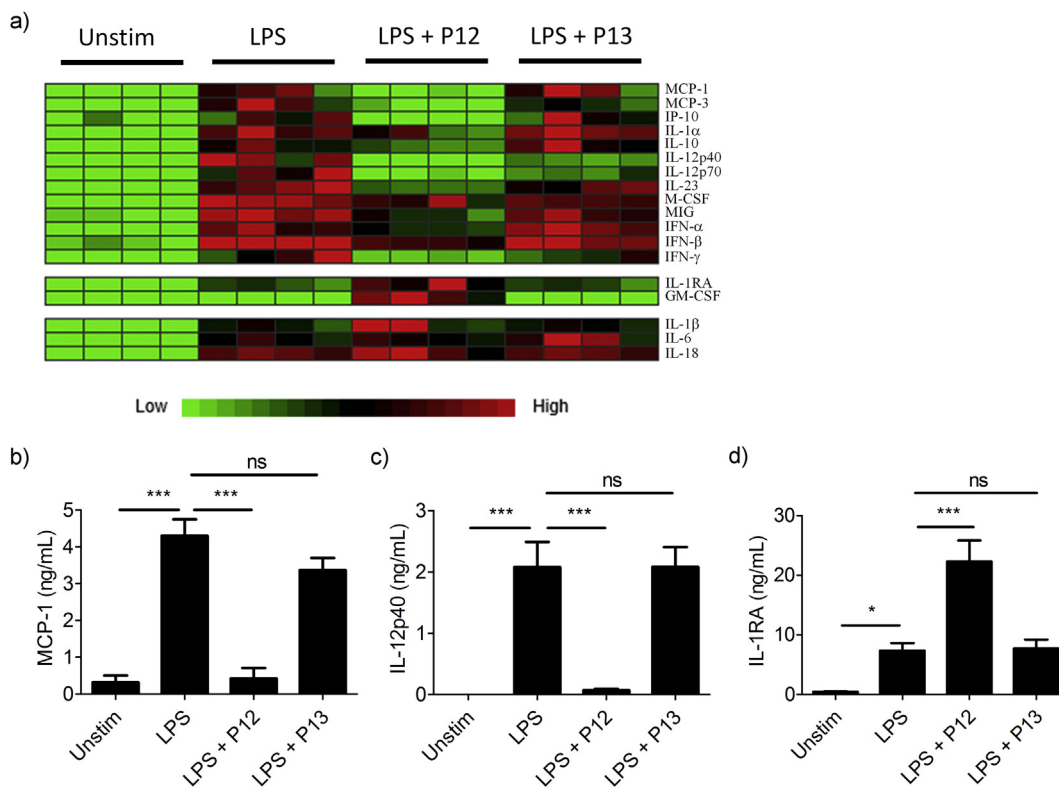


**Fig. 2.** Effect of the anti-inflammatory nanoparticle P12 treatment on the cytokine production profile of LPS-stimulated PBMC. (a) Heat map cytokine profiles from a multiplexed cytokine assay; top panel shows the cytokines significantly reduced by P12 ( $p < 0.05$  vs. LPS); middle panel shows cytokines were significantly increased by P12 ( $p < 0.05$  vs. LPS); bottom panel shows those cytokines that were not significantly changed. Selected cytokines (b) MCP-1, (c) IL12-p40 and (d) IL-1RA were independently confirmed by ELISA. \* $p < 0.05$ , \*\*\* $p < 0.001$ , ns: not significant,  $n = 4$ .

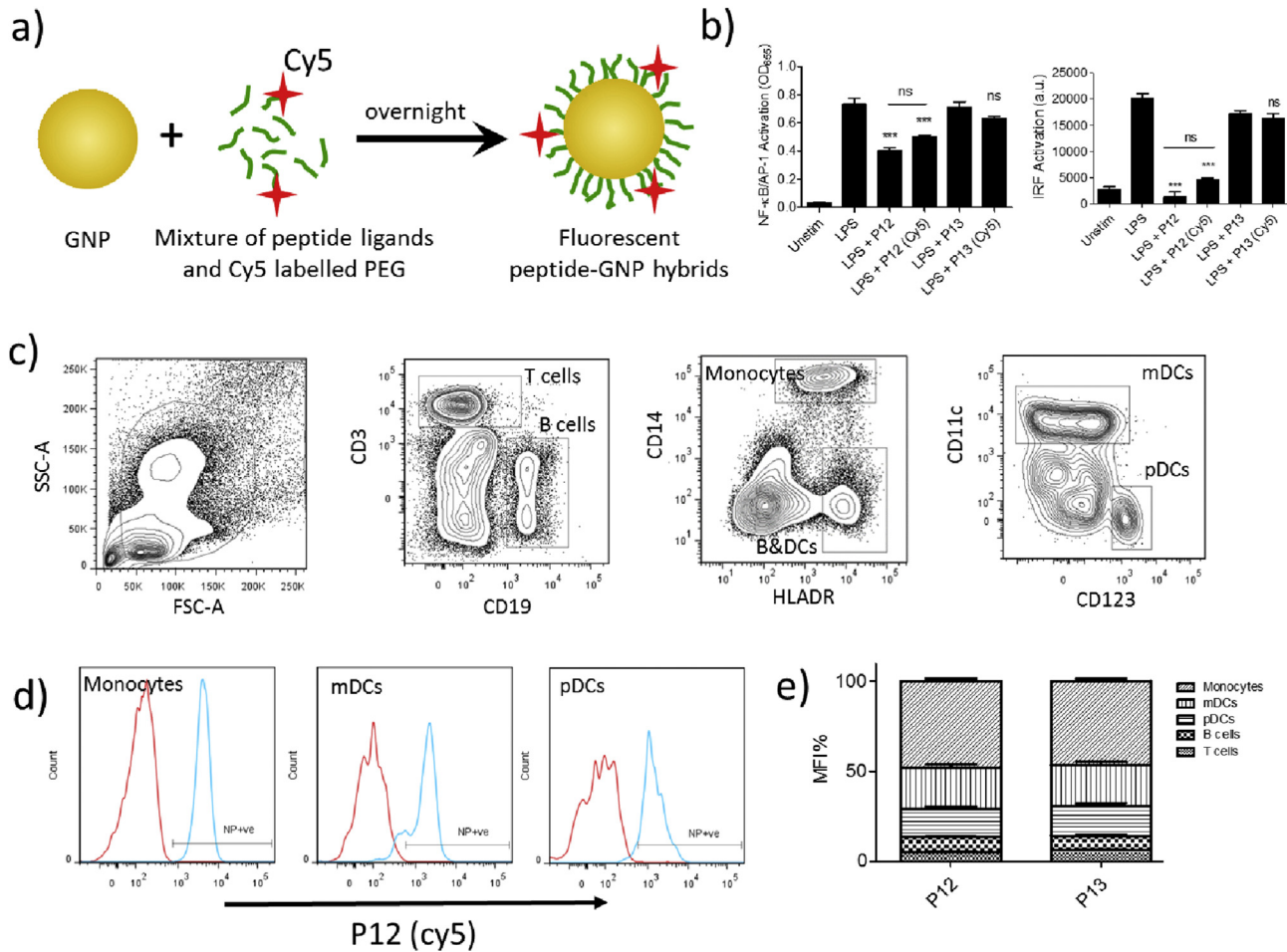


**Fig. 3.** Identification of the immune cells in the PBMC population targeted by the anti-inflammatory nanoparticles using multi-parameter flow cytometry analysis. (a) Construction of the fluorescent nanoparticles. (b) Anti-inflammatory activity of fluorescent P12 and P13 nanoparticles. \*\*\* $p < 0.001$ , ns: not significant,  $n = 3$ . (c) Gating strategy to identify specific immune cells within the PBMC population. (d) Uptake of P12 nanoparticle by phagocytic immune cells, including monocytes, mDCs and pDCs. (e) Distribution of internalized P12 and P13 nanoparticles in specific immune cells. ns: not significant.

higher pH [28]. As shown in Fig. 6a, pHrodo red fluorescence (red) became much less bright with bafilomycin, chloroquine and P12 treatment in comparison with untreated cells and P13 treatment. The ratio of fluorescein to pHrodo red fluorescence was quantified (Fig. 6b). Compared to untreated cells, exposure to bafilomycin, chloroquine and P12 significantly increased the ratio from 2 to 5, 9 and 4, respectively, indicating an increase in endosomal pH; while P13 had no effect.

To further confirm that the blockade of endosomal acidification by P12 was due to its buffering capability, we performed a pH titration on both P12 and P13 at two different concentrations (20 nM and 5 nM) in comparison with 0.9% normal NaCl solution as a control. As shown in Fig. 6c, both P12 and P13 at a higher concentration of 20 nM showed a buffering effect between pH 4 and pH 6 compared to the control, whereas at a lower concentration of 5 nM, they did not exhibit such an effect. These findings were further validated on selected nanoparticle hybrids from Fig. 5 with low (SS), medium (WW) and high cellular uptake (LL) (Fig. S5). We found that the pH titration curves of SS- and LL-nanoparticles were similar to those of P12 (FF) and P13 (AA) at both concentrations of 5 nM and 20 nM. However, the WW-nanoparticle showed a stronger pH buffering effect, even at a lower concentration of 5 nM. These results provided two strong lines of evidence to support our hypothesis: (a) the peptide-decorated nanoparticle hybrids (P12

and P13) have a buffering effect in the endosomal pH range (pH 4.5–6); and (b) the pH buffering capacity of the hybrids depends on the nanoparticle concentration (i.e., the uptake quantity of nanoparticles in the endosome) and the type of amino acids displayed on the nanoparticle surface.

**Defining the anti-inflammatory mechanism(s) of action of P12.** The nanoparticle P12 had global anti-inflammatory effects on the transcriptome and cytokine production profiles of TLR4 signaling (Figs. 1 and 2, Table 1). At the cellular level, P12 was taken up at high levels by phagocytic immune cells wherein it prevents physiological endosomal acidification (Figs. 3–6). Based on these findings, we propose a hypothetical working model for the anti-inflammatory activity of P12 (Fig. 7a), which predicts that blockade of endosomal acidification inhibits downstream TLR4 signaling pathways, leading to the reduction of NF- $\kappa$ B, IRF3 and MAPK activation.

To link attenuation of endosomal acidification to the inhibition of TLR4 signaling, we tested the effect of these employed endosomal pH modulators, CQ and BAF, using reporter cell systems that provide a read-out of both arms of the TLR4 pathway (i.e. NF- $\kappa$ B and IRF). As shown in Fig. 7b, the pH modulators (bafilomycin and chloroquine) were all effective in inhibiting IRF activation, the TRIF-dependent arm of TLR4 signaling that is associated with endosomes. Interestingly, only chloroquine but not bafilomycin was able

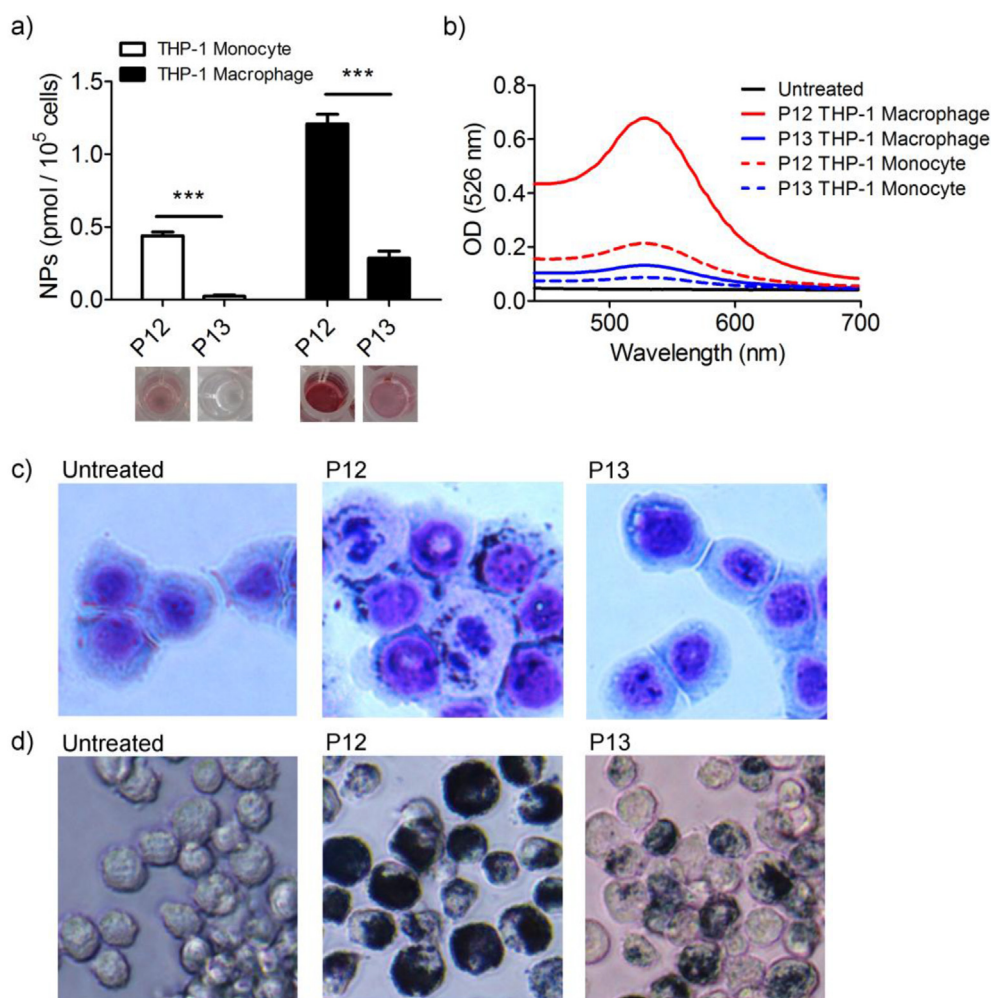


**Fig. 4. Cellular uptake of P12 and P13 nanoparticles in phagocytic immune cells.** (a) Quantitative uptake of nanoparticles P12 and P13 in THP-1 monocytes and THP-1 derived macrophages. \*\*\* $p < 0.001$ ,  $n = 4$ . (b) UV–Vis spectra of extracted internalized nanoparticles from THP-1 macrophages and THP-1 monocytes. (c and d) Representative microscopic images of THP-1 monocytic cells (c) and THP-1 derived macrophages (d). Cells were treated with nanoparticles P12 and P13 for 24 h; images were taken at  $200\times$  magnification.

to inhibit LPS-induced NF- $\kappa$ B activation (the MyD88-dependent arm), probably due to their different mechanisms of action (buffering effect vs. V-ATPase inhibitor) (Fig. 7c). This working model also predicted that pH modulators would inhibit other endosomal-based signaling cascades, such as TLR3 signaling. As shown in Fig. 7b and c, following exposure to the TLR3 ligand, poly I:C, both NF- $\kappa$ B and IRF activation were suppressed by chloroquine and P12 treatment, but not by P13. Furthermore, using immunoblotting we confirmed that P12 treatment suppressed TLR3 and TLR4 signaling as demonstrated by a reduction of p65 phosphorylation,  $\kappa$ B $\alpha$  degradation, IRF3 phosphorylation, and phosphorylation of p38, ERK1/2 and JNK (Fig. S6). In contrast to TLR3 and TLR4, signaling through the extracellular surface receptor IL-1R was not affected by pH modulators nor nanoparticle treatment (Fig. 7d and e). These results indicate that modulation of endosomal pH by P12 inhibits TLR responses originating in the endosome. Taken together, these data demonstrate that the high cellular uptake and attenuation of the endosomal pH likely play an important role in the inhibitory activity of P12, and that the inhibitory activity is determined by the peptides decorated on the nanoparticle surface (P12 vs. P13 and Fig. 5).

**In vivo therapeutic efficacy of the anti-inflammatory nanoparticles.** To further explore the clinical translational potential of

our anti-inflammatory nanoparticles, we evaluated the impact of P12 in a murine model of intestinal inflammation that mimics human inflammatory bowel disease (IBD). An IBD model was a compelling choice for *in vivo* evaluation of P12 for a number of reasons. First, inappropriate initiation and perpetuation of inflammatory responses to commensal microorganisms and danger signals in the gut is central to the pathogenesis of IBD [29], and targeting TLR signaling is predicted to be beneficial for improving the outcomes for patients with IBD [30]. Second, a number of the inflammatory pathways specifically targeted by P12 (see Table 1) have been implicated in the pathogenesis of IBD [24,31]. Third, P12 primarily targets phagocytic immune cells, which are key mediators in maintaining mucosal and commensal homeostasis in the intestine [32].

The dextran sulfate sodium (DSS)-induced colitis mouse model was used to evaluate the therapeutic efficacy of P12. It was found that intraperitoneal injection of P12 (1.5 mg/dose given every second day from Day -1 to Day 5), significantly reduced a number of key features of intestinal inflammation in comparison to control groups treated with either the inactive nanoparticle (P13) or PBS (as an injection control). Specifically, mice treated with P12 lost less body weight (Fig. 8a), had better overall disease activity indices (Fig. 8b) and stool consistency (Fig. 8c), and had less inflammation

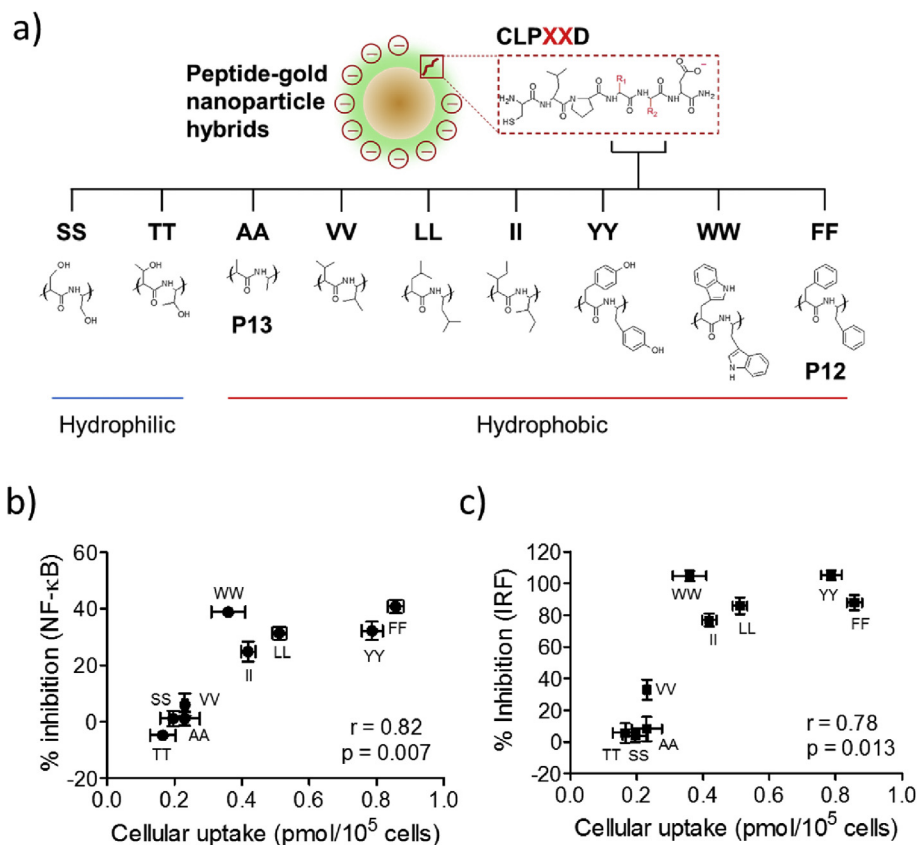


**Fig. 5. The relationship between the cellular uptake of various peptide-GNP hybrids and their anti-inflammatory activity.** (a) A scheme showing the amino acid sequences of the peptides conjugated on the GNP surface. The middle XX region could be amino acids with hydrophilic side chains such as serine (SS) and threonine (TT), or hydrophobic side chains, such as alanine (AA, P13), valine (VV), leucine (LL), isoleucine (II), tyrosine (YY), tryptophan (WW), or phenylalanine (FF, P12). (b–c) Correlation of the cellular uptake of various peptide-GNP hybrids and their inhibitory activity on NF-κB (b) and IRF (c) pathways of TLR4 signaling in THP-1 reporter cells derived macrophages. Correlation coefficient ( $r$ ) is equal to 0.82 ( $p = 0.007$ ) for NF-κB inhibition and 0.78 ( $p = 0.013$ ) for IRF inhibition;  $n = 4–5$ .

in the colon (Fig. 8d and e). These data confirm that P12 is effective in reducing inflammation in an *in vivo* model of intestinal inflammation.

## 2. Discussion

**Nanoparticle-based inhibitors of TLR signaling as a next generation of anti-inflammatory therapeutics.** TLR signaling plays a central role in the pathophysiology of many acute and chronic human inflammatory diseases [3]. Inhibitors and antagonists that down-regulate excessive TLR signaling are predicted to be beneficial in controlling damaging inflammation in these inflammatory conditions [5]. Currently, only a few TLR inhibitors/antagonists have been developed for clinical use, mainly targeting TLR4 signaling for the treatment of sepsis [4,33]. These are either small molecules or antibodies developed to specifically block the interaction between the receptor and the pathogenic ligands, or to inhibit specific downstream signaling molecules [34,35]. However, they show limited therapeutic benefit in treating severe sepsis, perhaps due to the immune complexity of sepsis. Given the redundancy of immune recognition and the fact that multiple pattern recognition receptor (PRR) pathways are often involved in responding to any infection, blocking one single pathway may not be sufficient to ameliorate established disease. To address this challenge, we have developed a nanomedicine that inhibits a broad range of TLR responses [22]. Very recently, a lipoprotein-like nanoparticle was designed to inhibit TLR4 signaling by scavenging and neutralizing LPS toxin [36].

Here, we characterized a novel nanoparticle-based TLR inhibitor that displayed potent anti-inflammatory activity (Figs. 1 and 2). In contrast to other small molecule inhibitors, the inhibitory activity of the nanoparticles was enabled by their polyvalent anionic nature and specific surface chemistry, and this inhibitory activity can be deliberately programmed by modifying the peptides decorated on the surface of the nanoparticles (Fig. 5) [22]. For example, replacing only two phenylalanine residues in P12 with alanine generates the biologically-inactive nanoparticle, P13. These anti-inflammatory nanoparticles also had a number of other beneficial features that make them attractive immune modulators. First, the nanoparticles preferentially targeted phagocytic innate immune cells (monocytes, macrophages and dendritic cells) (Fig. 3) that play a key role in inflammatory responses. Using the P12 “nano-drug” to target phagocytic innate immune cells is anticipated to enhance their therapeutic effect by acting on the primary mediators of inflammatory responses, while reducing the potential side effects on other non-disease causing cells. Second, the lead nanoparticle P12 was able to inhibit multiple inflammatory signaling pathways, including multiple TLR pathways (TLR4 and TLR3), cytokine signaling and interferon signaling pathways (Table 1). This broader inhibitory activity may be beneficial for managing excessive inflammation, which is generally triggered through multiple, redundant defense pathways present within the immune system. Although these rationally-designed anti-inflammatory nanoparticles show great promise in reducing damaging inflammation, they also have some limitations. For example, P12 is based on a gold nanoparticle core that is not biodegradable and may cause

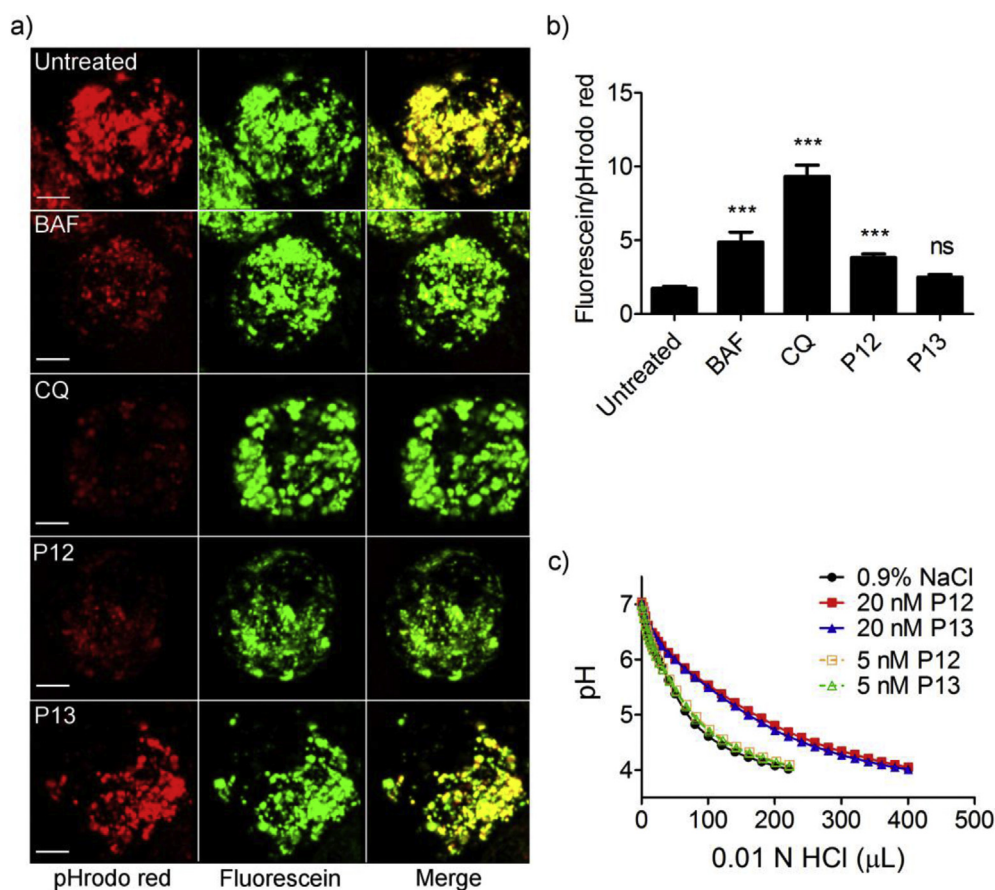


**Fig. 6. Modulation of endosomal pH by the anti-inflammatory nanoparticle P12.** (a) Confocal images of THP-1 derived macrophages treated with the nanoparticles and known pH modulators, bafilomycin (BAF) and chloroquine (CQ). Scale bar represents 4  $\mu\text{m}$ . Endosomal pH was probed with pHrodo red-dextran (red) and fluorescein-dextran (green). (b) Quantitative ratios of green-to-red signals as indicators of endosomal pH. \*\*\* $p < 0.001$ ; ns: not significant,  $n = 20\text{--}30$  cells from 3 independent experiments. (c) pH titration of different concentrations of P12 and P13 in normal saline (0.9% NaCl). (For interpretation of the references to colour in this figure legend, the reader is referred to the web version of this article.)

challenges with repeated, long-term administration. Advancing these nanomedicines to clinical application will require biodegradable nanoparticles, given concerns about bioaccumulation of gold nanoparticles.

**The anti-inflammatory nanoparticle targets endosomes to modulate TLR signaling.** Mounting evidence now identifies endosomes as much more than a cellular ‘sink’ for degrading and recycling cell surface receptors to terminate signaling. Endosomes are recognized as essential sites for signal transduction. Receptors transmit different signals from endosomes than from the cell surface, driving distinct physiological responses [7,8]. Therefore, selectively manipulating endosomal receptor signaling offers new options for therapeutic intervention.

The anti-inflammatory nanoparticle, P12, primarily targets endosomal signaling due to the specific peptide coating that facilitates high levels of endosomal uptake (Fig. 4) [20,21]. Following accumulation in the endosomal compartment, P12 prevented normal physiological endosomal acidification, thus inhibiting downstream TLR-initiated signaling (Figs. 6 and 7). It has been found that the endosomal trafficking of endocytosed LPS leads to termination of the MyD88-dependent signal [9]. In the case of P12 (vs. P13), its high level of endosomal uptake might have facilitated the endocytosis process, which in turn would be anticipated to shut down the MyD88-dependent pathway of TLR4 signaling. In addition, endosomal pH plays an important role in regulating endosomal TLR signaling, including signaling through TLR3, TLR4, TLR7/

8, and TLR9 [25–27]. Our results demonstrated that the blockade of endosomal acidification by P12 indeed inhibited TLR3 and TLR4 signaling, but not the extracellular receptor signaling of IL-1R (Fig. 7). This model is consistent with our observation that the endosomal pH modulators, bafilomycin and chloroquine, attenuated the MyD88-independent (TRIF-dependent) signaling pathway (Fig. 7b). Chloroquine, a weak base that can partition into endosomes and perturb the pH, attenuated both MyD88-independent and MyD88-dependent pathways (Fig. 7b and c); however, bafilomycin, a V-type ATPase proton pump inhibitor, only inhibited MyD88-independent signaling. Interestingly, the anti-inflammatory nanoparticle P12 behaved similarly to chloroquine, suggesting that they may share some similar mechanisms. This mechanistic similarity may be due to the negative charge of the aspartate (with side chain pKa of  $\sim 3.9$ ) on the P12 nanoparticles (Fig. 6c) sequestering protons and preventing normal endosomal acidification. Although we have strong evidence to establish that P12 targeted the endosome of phagocytic cells to suppress inflammation, we cannot rule out the possibility of P12 acts on other plasma membrane proteins or autophagosome-mediated immune signaling [37,38]. These are all very encouraging evidence showing the translational potential of the peptide-GNP hybrids as a promising, next generation anti-inflammatory therapeutics.

**The promise of anti-inflammatory nanoparticles for treating inflammatory disease.** Since the “nano-drug” P12 exhibited a

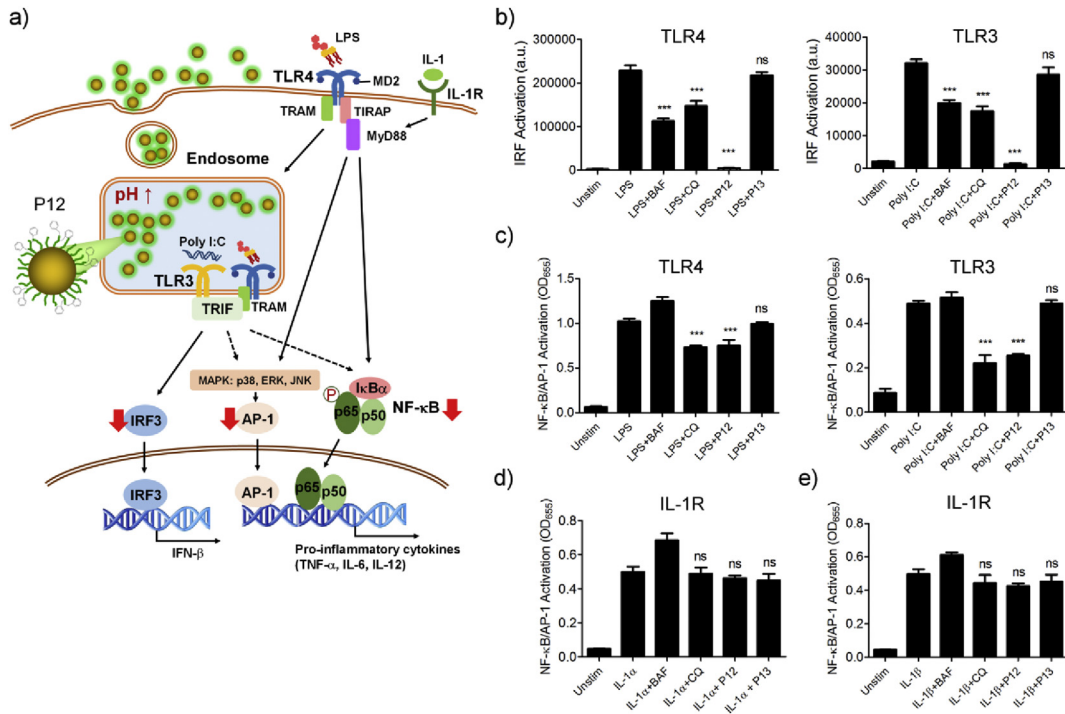


**Fig. 7. Proposed mechanisms of action of the anti-inflammatory nanoparticle P12 by blocking endosomal acidification.** (a) Illustration of the proposed mechanisms of action of the nanoparticle P12 on TLR signaling. (b–c) Effect of endosomal pH modulators and nanoparticles on the IRF activation (b) and NF-κB activation (c) in TLR3 (right) and TLR4 (left) signaling in THP-1 derived macrophages. (d–e) Effect of endosomal pH modulators and nanoparticles on the NF-κB activation in IL-1R signaling with IL-1α (d) and IL-1β (e) stimulation in THP-1 derived macrophages. \*\*\*p < 0.001, ns: not significant, n = 3–4.

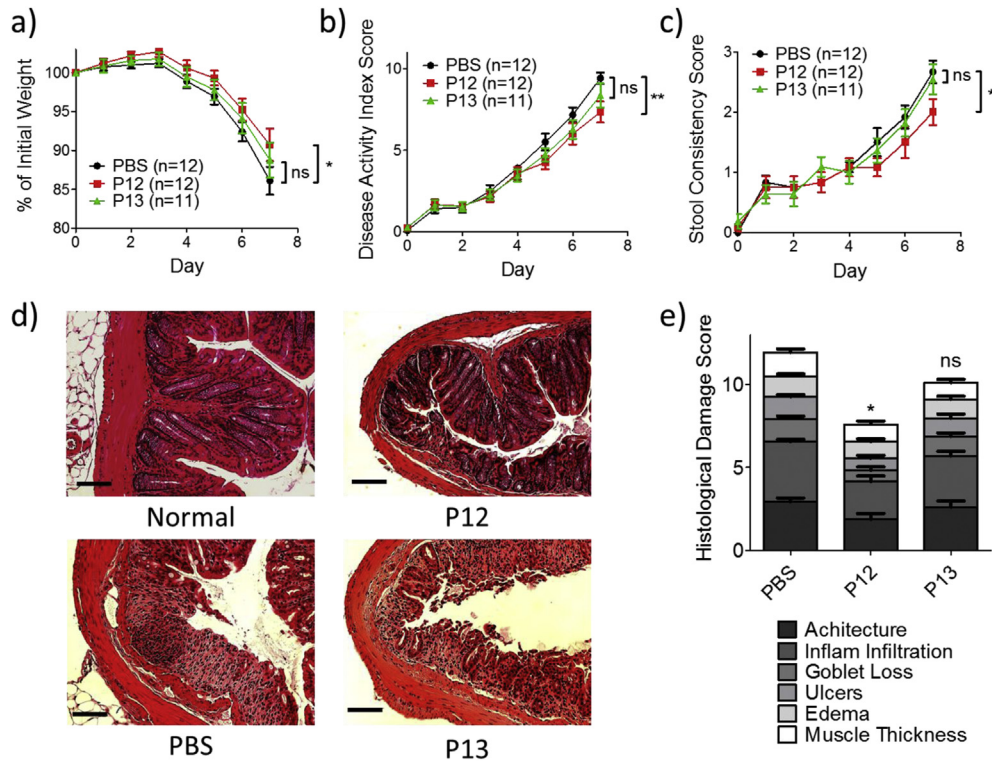


**Fig. 8. Evaluation of the therapeutic efficacy of nanoparticle P12 in the DSS-induced mouse model of intestinal inflammation.** Nanoparticle P12 treatment improved the disease severity and dampened intestinal inflammation, as indicated by: reduced weight loss (a), disease activity indices (b), stool consistency (c), H&E stained colon sections (d) and histological damage scores (e). Scale bar = 100 μm; \*p < 0.05; \*\*p < 0.01; ns: not significant.

broad spectrum of anti-inflammatory activity, it holds promise for treating inflammatory diseases with complex underlying pathophysiology. Among the broad array of human inflammatory disorders, inflammatory bowel disease (IBD), encompassing Crohn's disease and ulcerative colitis, is a particularly burdensome idiopathic condition that predominantly affects the gastrointestinal tract. The pathogenesis of IBD is not fully understood, but involves a complex interplay of genetic, environmental and immunological factors [39,40]. Growing evidence has implicated aberrant recognition by PRRs of commensal microbiota, and/or products from tissue damage in the gut, as playing a central role in the pathogenesis of IBD [41–43]. Therefore, reducing innate inflammatory responses is predicted to be a useful strategy to suppress harmful inflammation in IBD.

We had anticipated that P12 would be a beneficial therapy in IBD because it targets key elements in the pathophysiology of the disease (Figs. 2 and 7, Table 1). For example, by inhibiting both MyD88-independent and -dependent TLR4 signaling (Fig. 7) [22], P12 significantly decreased LPS-induced production of chemotactic and pro-inflammatory cytokines (e.g., MCP-1, MCP-3, IL-12p40, IL-23 and interferons) implicated in IBD (Fig. 2) [31,44]. Moreover, our transcriptomic data revealed that P12 inhibited multiple signaling pathways involved in the pathogenesis of IBD, including TLRs, interferon, TNF and JAK-STAT signaling (Table 1) [23,24]. Finally, P12 had mechanistic similarities to chloroquine which has shown beneficial activity in IBD (Fig. 7) [45,46].

### 3. Conclusions

Building upon our earlier discovery on a novel class of anti-inflammatory nanoparticles [22], we have made significant progress in demonstrating that the anti-inflammatory effects are highly dependent on the peptide coatings on the nanoparticle surface, and advancing this nanomedicine towards clinical application. Specifically, we found that the anti-inflammatory nanoparticle P12 targeted phagocytic immune cells where it suppressed inflammation by blocking the endosomal acidification resulting from its high cellular uptake and pH buffering capacity. Globally, P12 reversed a large portion of LPS-stimulated transcriptomic changes, inhibited a number of key inflammatory pathways (TLR, PKR, interferon, TNF, chemokine and JAK-STAT signaling), and suppressed the secretion of multiple pro-inflammatory chemokines and cytokines. Furthermore, in a mouse model of intestinal inflammation, P12 improved colonic inflammation *in vivo*. In contrast, the nanoparticle P13 derived from P12 (with only two amino acids difference in the decorating peptides) was biologically inactive. We anticipate that this nanoparticle-based anti-inflammatory approach will empower an exciting, new area of investigation to design and develop immunotherapeutics for treating human inflammatory diseases.

### 4. Methods

**Gold nanoparticle synthesis and preparation of peptide-GNP hybrids.** Gold nanoparticles (GNPs) were synthesized according to a modified procedure from the literature and our earlier work [22,47]. The synthesized GNPs have an average diameter of 13 nm determined by Hitachi H-7000 electron microscope (Tokyo, Japan) at an accelerating voltage of 200 kV. The fabrication of peptide-GNP hybrids was conducted following our published protocol [20–22]. In brief, peptides (from CanPeptide Inc., Montreal, Canada) were dissolved in endotoxin free, ultrapure water as a stock solution of 1 mM. The hybrids were prepared by mixing one volume of peptide stock solutions with ten volume of the synthesized 13 nm GNP solution (final concentration of GNPs is ~11 nM). After overnight incubation, all peptide-GNP hybrids were filtered through a syringe

filter (0.22  $\mu$ m, Milipore, Billerica, MA, USA), following by centrifugation (14,000 rpm at 4 °C for 30 min) and washing 3 times with sterile phosphate buffered saline (PBS, HyClone, GE Healthcare) to remove free peptide ligands.

**PBMC isolation.** PBMC were isolated from peripheral blood of healthy volunteers using density gradient centrifugation on Ficoll-Paque™ Plus (GE Healthcare). The protocol was approved by the University of British Columbia Clinical Research Ethics Board (H04-034). Isolated PBMC were washed twice with PBS and resuspended in a complete RPMI-1640 medium containing 10% fetal bovine serum (FBS), 2 mM L-glutamine (all from HyClone, GE Healthcare) and 1 mM sodium pyruvate (Invitrogen). PBMC were plated in a 24-well plate at a density of  $2 \times 10^6$  cells/well and  $5 \times 10^5$  cells/well in 0.5 ml medium for RNA extraction and cytokine analysis, respectively; cells were then rested for 1 h prior to further stimulation by LPS with or without the peptide-GNP hybrids treatments.

**RNA extraction and cDNA library preparation for RNA-Seq.** Total RNA of PBMC were extracted using RNeasy mini kit (Qiagen, Valencia, CA, USA) according to the manufacturer's instructions. Total RNA concentrations were determined using a Nanodrop ND-100 Spectrophotometer (Nanodrop Technologies, Wilmington, DE, USA). The RNA quality was evaluated using Agilent 2100 Bioanalyzer (Agilent Technologies, Santa Clara, CA, USA). For RNA-Seq analysis, RNA libraries were created from each samples using NEB Next Ultra Directional RNA Library preparation kit from Illumina (Illumina, San Diego, CA, USA) following the company recommended protocol.

**RNA-Seq and transcriptomic analysis.** RNA-Seq was performed on an Illumina GA IIX instrument using single end reads followed by de-multiplexing using CASAVA. Sequencing quality was assessed based on GC content, average base quality and Illumina adapter contamination using FastQC. Reads were mapped to the human genome (hg19) using Tophat2, sorted and indexed using Samtools and counted using HTseq. To establish a signature gene expression profile that was representative of nanoparticle activity, DESeq2 was used to identify genes that had statistically significant differential expression (FDR<0.1) in four comparisons: between LPS and control, between P13 and control, between LPS and P12 and between P12 and P13; and that were not significantly different (FDR>0.1) in two comparisons: between P12 and control and between P13 and LPS. Pathway analysis was performed on this signature gene expression profile using the Sigora R package to identify unique pathways based on over-representation of gene-pairs (this method limits the appearance of set of genes in multiple overlapping pathways, selecting only the most significantly dysregulated pathways). To look at the global changes in gene expression in response to each stimulus individually, DESeq2 was used to make pairwise comparisons with a FDR threshold of 0.05 and fold change cut off of 2. These gene lists were plotted in Venn diagrams using BioVenn.

**Cytokine analysis.** PBMC were stimulated with LPS in the presence or absence of the nanoparticle hybrids (100 nM) and incubated for 24 h. Culture media were centrifuged at 5000 rpm with a bench-top refrigerated microcentrifuge (microfuge 22R, Beckman Coulter, Indianapolis, IN) at 4 °C for 5 min to remove cells and the supernatants were further centrifuged at 14,000 rpm at 4 °C for 30 min. Supernatants were collected and stored at –80 °C prior to the cytokine measurements by Luminex-based Procarta custom 23-plex assay (eBioscience, San Diego, CA). Selected cytokines were further validated by ELISA (human ELISA Ready-Set Go kits, eBioscience), following the manufacturer's protocol.

For the Luminex assay, supernatants were diluted 1:1 and 1:10 in RPMI medium for the measurements, and the assay were performed according the manufacturer's protocol. Assays were read on

a Luminex 200 total system running MasterPlex (MiraiBio) software. The 23 cytokines quantified in the assay included: GM-CSF, IL-10, IFN- $\alpha$ 2, IL-1 $\beta$ , TNF- $\alpha$ , IL-23, IL12-p70, TNF- $\beta$ , IL-6, IL-1RA, IL12-p40, IFN- $\gamma$ , IL-9, IP-10 (CXCL10), MIP-1 $\beta$  (CCL4), GRO- $\alpha$  (CXCL1), MCP-1 (CCL2), ENA78 (CXCL5), MCP-3 (CCL7), M-CSF, IL-8 (CXCL8), and MIG (CXCL9). Mean Fluorescence intensity of the samples was interpolated from the standard curves to analyte quantity using five-parameter logistical fit.

**Immuno-phenotyping with flow cytometry.** We used a polychromatic flow cytometric assay to identify T cells, B cells, monocytes, mDCs and pDCs in PBMC. The antibodies used include HLA-DR (clone TU36; BD Biosciences), CD14 (clone 61D3; BD Biosciences), CD123 (clone 6H6; eBioscience), CD11c (clone B-ly6; BD Biosciences), CD3 (clone UCHT1; BD Biosciences) and CD19 (clone SJ25C1; BD Biosciences). A fixable viability dye (eFluor 450; eBioscience) was used to exclude dead cells from the analysis. The data were collected on a LSRII flow cytometer (BD Biosciences) and analyzed using the FlowJo software (Tree Star, Inc., Ashland, OR, USA).

**Nanoparticle cellular uptake assay.** THP-1 cell derived macrophages ( $1 \times 10^6$  cells/ml) using phorbol-12-myristate-13-acetate (PMA, 100 ng/ml, Sigma Aldrich) were seeded in a 24-well plate (0.6 ml/well). Cells were treated with the nanoparticle hybrids (100 nM) for 24 h. After washing three times with ice cold PBS, cells were lysed in lysis buffer containing 0.1 N NaOH and 0.5% Triton for 0.5 h. Cell lysates were diluted with PBS for UV–Vis absorption measurement at 526 nm. A calibration curve was generated for each hybrid by acquiring the hybrid absorbance in PBS with known concentrations. The nanoparticle uptake was calculated as pmol of nanoparticles per 100,000 cells according to the calibration curve.

**Intracellular pH assay and confocal imaging.** THP-1 cell derived macrophages seeded in 8-well chamber slides (Nunc Lab-Tek, Sigma-Aldrich, Oakville, Canada) were incubated for 6 h with a mixture of fluorescein- and pHrodo red-labeled 10,000 MW dextrans (10  $\mu$ g/ml) (Life Technologies). Cells were then washed with PBS three times, and treated with bafilomycin A1 (100 nM), chloroquine (50  $\mu$ M), P12 (100 nM) or P13 (100 nM) for 1 h. Cells were then washed with PBS three times and imaged on a confocal microscope (Leica SP5). Fluorescein (excitation 488/emission 525) and pHrodo red (excitation 565/emission 585) fluorescence within intracellular vesicles were quantified by intensities across line profiles. Background was subtracted, and the ratio of fluorescein to pHrodo red fluorescence was calculated and reported. For each treatment, a minimum of 20 cells from three independent experiments were analyzed.

**Acid-base titration of the peptide-GNP hybrids.** The buffering effect of the hybrids P12 and P13 was determined by a standard acid-base titration method using a benchtop pH meter (Accumet AB15, Fisher-Thermo Scientific) [48]. P12 and P13 hybrids at two different concentrations of 20 nM and 5 nM were re-suspended in a 0.9% NaCl solution, and the 0.9% NaCl solution was used as the control. All solutions (15 ml) were first adjusted to pH 7 with 0.1 N NaOH, and were then titrated by stepwise addition (1–20  $\mu$ l) of 0.01 N HCl solution until pH 4 was reached. The titration profile was obtained by plotting the pH value vs. total volume of HCl added.

**Reporter cell assays for the analysis of NF- $\kappa$ B/AP-1 and IRF activation.** THP1-XBlue™ and THP1-Dual™ cells were purchased from InvivoGen (San Diego, CA, USA). The reporter cells were cultured as recommended by the supplier using standard protocols. THP-1 reporter cells were differentiated into a macrophage-like phenotype using 50 ng/ml PMA for 24 h at a density of  $1 \times 10^5$  cells/well in 100  $\mu$ l in a 96-well plate. Cells were washed with PBS and allowed to rest for two days prior to TLR stimulation and nanoparticle hybrid treatments. After 24 h treatment, culture media were collected and centrifuged at 14,000 rpm (microfuge

22R, Beckman Coulter) at 4 °C for 30 min, and stored at –20 °C for assays.

To measure NF- $\kappa$ B/AP-1 activation, the supernatants (20  $\mu$ l) from THP1-XBlue™ cells were incubated with QUANTI-Blue solution (180  $\mu$ l) (InvivoGen) at 37 °C for 1–2 h to allow color development. The color change of the substrate solution was quantified by optical density measurement at 655 nm on a SpectraMax 384 Plus plate reader (Molecular Devices, Sunnyvale, CA, USA). For the analysis of IRF activation, the supernatants (10  $\mu$ l) from THP1-Dual™ cells transferred into a 96-well white plate (flat-bottom) and the luciferase activities were measured using a luminometer (TECAN, Weymouth, UK) by auto-injection of QUANTI-Luc assay solution (50  $\mu$ l per well) (InvivoGen).

**Immunoblotting.** THP-1 cells were seeded in a 12-well plate (at a density of  $2 \times 10^6$  cells/well), and differentiated using 100 ng/ml PMA for 72 h. Cells were washed with PBS and allowed to rest for three days prior to stimulation and hybrid treatments over time (0–4 h). Cells were lysed in a modified RIPA buffer supplemented with Halt protease and phosphatase inhibitor cocktail (Thermo Scientific). The total protein concentrations of the lysates were measured and adjusted to the same concentration. Lysates were resolved by electrophoreses on 10% SDS-polyacrylamide gels and transferred onto PVDF membranes (Immobilon FL, Millipore). Blots were blocked with 5% bovine serum albumin in tris-buffered saline (G Biosciences) containing 0.1% TWEEN 20 (Calbiochem) for 1 h at room temperature. The blots were stained with primary antibodies against phospho-p65, I $\kappa$ B $\alpha$ ,  $\beta$ -actin, phospho-p38, phospho-JNK, GAPDH (all from Cell Signaling Technology), phospho-ERK1/2 (Thermo Fisher Scientific), and phospho-IRF3 (Santa Cruz) overnight at 4 °C. Blots were subsequently washed and stained with fluorescently-labeled secondary antibodies, IRDye 680LT and 800CW (LI-COR Biosciences) for 1 h. Blots were imaged and quantified on a LI-COR Odyssey infrared imaging system (LI-COR Biosciences).

**DSS-induced intestinal inflammation murine model.** 8–9 week old C57BL/6 mice were used for DSS-induced colitis experiments. Mice were housed at the Child & Family Research Institute (Vancouver, Canada) in a specific pathogen and Helicobacter free barrier facility. Experiments were performed according to institutional and Canadian Council on Animal Care guidelines (A13-0054). 2.75% DSS (MW 36–50 000; MP Biomedicals, Solon, OH, USA) was dissolved in drinking water and given to mice *ad libitum* for 7 days.

Nanoparticle treatments (P12 and P13 at concentration of 1  $\mu$ M) or PBS control, each at a total volume of 100  $\mu$ l and 100 pmol nanoparticles per mouse, were given via intraperitoneal injection (ip) as a pre-treatment 1 day prior to start of DSS, followed by every second day of the experiment thereafter. Daily disease activity indices (DAI) were taken, including weight loss, stool consistency, and rectal bleeding scores. Scores were assigned on a scale of 0–4 as follows: for weight loss: 0 < 1%, 1 = 1–3%, 2 = 3–6%, 3 = 6–9%, and 4 > 9%; rectal bleeding: 0 = no blood in stool, 1 = blood detectable on hemocult paper (Beckman Coulter, Mississauga, Canada), 2 = blood visible in stool, 3 = extensive blood in stool, and 4 = blood in stool and around anus; stool consistency: 0 = normal, 1 = loose, 2 = very loose, 3 = diarrhea, and 4 = no visible pellets. Combined scores for each of the parameters represent the DAI for each mouse. Colon lengths were measured and pictures were taken upon autopsy.

To assess histological damage, excised colons were fixed in PBS-buffered 10% formalin (Fisher Scientific, Ottawa, Canada). Fixed colons were then embedded in paraffin, cross-sectioned, and stained with hematoxylin and eosin (H&E) by the histology core facility at the Child & Family Research Institute. Histological damage scores were assigned by two individuals blinded to the experimental conditions and averaged. The 16 point damage scores were

combined for each mouse as follows: for loss of architecture: 0 = none, 1 < 25% loss, 2 = 25%–50% loss, 3 = 50–75% loss, 4 > 75% loss; immune cell infiltration: 0 = none, 1 = occasional immune cell in lamina propria, 2 = increased immune cells in lamina propria, 3 = confluent immune cells in lamina propria and breaching mucosa, and 4 = immune cell infiltration throughout the section; goblet cell depletion: 0 = none, 1 < 50% depletion, and 2 > 50% depletion; ulceration: 0 = none, 1 = intermediate ulceration, and 2 = substantial ulceration; edema: 0 = none, 1 < 50% of section, and 2 > 50% of section; muscle thickening: 0 = none, 1 = intermediate thickening, and 2 = substantial thickening.

**Statistical analysis.** Data were analyzed as means  $\pm$  standard errors of the means (SEM). Statistical significance was assessed by performing one- or two-way ANOVA and the Bonferroni post-test, as applicable. Analyses were performed by using Prism 5 software (GraphPad). Statistical significance was determined by the P values using the following annotation: \* < 0.05, \*\* < 0.01, or \*\*\* < 0.001 throughout the figures.

**Supporting Information Available:** Additional figures describing hierarchical clustering of samples with FactoMineR analysis, gene expression profiles of LPS responsive genes that are inhibited by P12 but not P13, gene ontology term enrichment for the biological process category of P12 altered LPS responsive gene expression, viability of P12 and P13 treated THP-1 cell derived macrophages, confirmation of the localization of P12 and P13 in endosomes, pH titration profiles of selected peptide-GNP hybrids, and the P12 altered TLR3 and 4 endosomal signaling pathway by immunoblotting are available free of charge via the Internet at <http://pubs.acs.org>.

## Acknowledgements

The financial support for this project was provided by grants to S.E.T. from Cystic Fibrosis Canada (CF Canada), Natural Sciences and Engineering Research Council of Canada (NSERC) and the Crohn's and Colitis Foundation of Canada (CCFC), by grants to M.L. and R.E.W.H. from the Canadian Institutes for Health Research (CIHR). S.E.T. holds the Aubrey J. Tingle Professorship in Pediatric Immunology and is a clinical scholar of the Michael Smith Foundation for Health Research. S.Y.F. was supported by a postdoctoral fellowship from the Child & Family Research Institute. T.R.K. is supported in part by a Career Award in the Biomedical Sciences from the Burroughs Wellcome Fund and a Michael Smith Foundation for Health Research Career Investigator Award. R.E.W.H. holds a Canada Research in Health and Genomics. H. Y. would like to acknowledge the support from The Program for Professor of Special Appointment (Eastern Scholar) at Shanghai Institutions of Higher Learning.

## Appendix A. Supplementary data

Supplementary data related to this article can be found at <http://dx.doi.org/10.1016/j.biomaterials.2016.09.032>.

## References

- [1] S. Akira, K. Takeda, Toll-like receptor signalling, *Nat. Rev. Immunol.* 4 (2004) 499–511.
- [2] L.A. O'Neill, C.E. Bryant, S.L. Doyle, Therapeutic targeting of toll-like receptors for infectious and inflammatory diseases and Cancer, *Pharmacol. Rev.* 61 (2009) 177–197.
- [3] L. Zuo, K. Lucas, C.A. Fortuna, C.C. Chuang, T.M. Best, Molecular regulation of toll-like receptors in asthma and COPD, *Front. Physiol.* 6 (2015) 312.
- [4] E.J. Hennessy, A.E. Parker, L.A. O'Neill, Targeting toll-like receptors: emerging therapeutics? *Nat. Rev. Drug Discov.* 9 (2010) 293–307.
- [5] G.F. Bezemer, S. Sagar, B.J. van, N.A. Georgiou, J. Garssen, A.D. Kraneveld, G. Folkerts, Dual role of toll-like receptors in asthma and chronic Obstructive pulmonary disease, *Pharmacol. Rev.* 64 (2012) 337–358.
- [6] S.M. Opal, P.F. Laterre, B. Francois, S.P. LaRosa, D.C. Angus, J.P. Mira, X. Wittebole, T. Dugernier, D. Perrotin, M. Tidswell, et al., Effect of eritoran, an antagonist of MD2-TLR4, on mortality in patients with severe sepsis: the ACCESS randomized trial, *JAMA* 309 (2013) 1154–1162.
- [7] J. Lee, I. Tattoli, K.A. Wojtal, S.R. Vavricka, D.J. Philpott, S.E. Girardin, Ph-dependent internalization of muramyl peptides from early endosomes enables Nod1 and Nod2 signaling, *J. Biol. Chem.* 284 (2009) 23818–23829.
- [8] J.E. Murphy, B.E. Padilla, B. Hasdemir, G.S. Cottrell, N.W. Bunnnett, Endosomes: a legitimate platform for the signaling train, *Proc. Natl. Acad. Sci. U. S. A.* 106 (2009) 17615–17622.
- [9] H. Husebye, O. Halaas, H. Stenmark, G. Tunheim, O. Sandanger, B. Bogen, A. Brech, E. Latz, T. Espevik, Endocytic pathways regulate toll-like receptor 4 signaling and link innate and adaptive immunity, *EMBO J.* 25 (2006) 683–692.
- [10] F. Chellat, Y. Merhi, A. Moreau, L.H. Yahia, Therapeutic potential of nanoparticulate systems for macrophage targeting, *Biomaterials* 26 (2005) 7260–7275.
- [11] F. Shima, T. Akagi, T. Uto, M. Akashi, Manipulating the antigen-specific immune response by the hydrophobicity of amphiphilic poly( $\gamma$ -glutamic acid) nanoparticles, *Biomaterials* 34 (2013) 9709–9716.
- [12] H. Takedatsu, K. Mitsuyama, T. Torimura, Nanomedicine and drug delivery strategies for treatment of inflammatory bowel disease, *World J. Gastroenterol.* 21 (2015) 11343–11352.
- [13] A. Ruiz-de-Angulo, A. Zabaleta, V. Gomez-Vallejo, J. Llop, J.C. Mareque-Rivas, Microdosed lipid-coated (67)Ga-Magnetite enhances antigen-specific immunity by image tracked delivery of antigen and CpG to lymph nodes, *ACS Nano* 10 (2016) 1602–1618.
- [14] S. Shaunak, S. Thomas, E. Gianasi, A. Godwin, E. Jones, I. Teo, K. Mireskandari, P. Luthert, R. Duncan, S. Patterson, et al., Polyvalent dendrimer glucosamine conjugates prevent scar tissue formation, *Nat. Biotech.* 22 (2004) 977–984.
- [15] T. Saxena, K.H. Loomis, S.B. Pai, L. Karumbaiah, E. Gaupp, K. Patil, R. Patkar, R.V. Bellamkonda, Nanocarrier-mediated inhibition of macrophage migration inhibitory factor attenuates secondary injury after spinal cord injury, *ACS Nano* 9 (2015) 1492–1505.
- [16] A.L. Siefert, M.J. Caplan, T.M. Fahmy, Artificial bacterial biomimetic nanoparticles synergize pathogen-associated molecular patterns for vaccine efficacy, *Biomaterials* 97 (2016) 85–96.
- [17] X. Xu, W. Ho, X. Zhang, N. Bertrand, O. Farokhzad, Cancer nanomedicine: from targeted delivery to combination therapy, *Trends Mol. Med.* 21 (2015) 223–232.
- [18] Z. Hunter, D.P. McCarthy, W.T. Yap, C.T. Harp, D.R. Getts, L.D. Shea, S.D. Miller, A biodegradable nanoparticle platform for the induction of antigen-specific immune tolerance for treatment of autoimmune disease, *ACS Nano* 8 (2014) 2148–2160.
- [19] L. Tang, J. Azzi, M. Kwon, M. Mounayar, R. Tong, Q. Yin, R. Moore, N. Skartsis, T.M. Fan, R. Abdi, et al., Immunosuppressive activity of size-controlled PEG-PLGA nanoparticles containing encapsulated cyclosporine, *J. Transpl.* (2012), 2012:896141.
- [20] H. Yang, S.-Y. Fung, M. Liu, Programming the cellular uptake of physiologically stable peptide–gold nanoparticle hybrids with single amino acids, *Angew. Chem. Int. Ed.* 50 (2011) 9643–9646.
- [21] H. Yang, Y. Zhou, S.Y. Fung, L. Wu, K. Tsai, R. Tan, T. Stuart, T. Machuca, M. de Perrot, T. Waddell, et al., Amino acid structure determines the immune responses generated by peptide-gold nanoparticle hybrids, *Part. Part. Syst. Charact.* 30 (2013) 1039–1043.
- [22] H. Yang, S.Y. Fung, S. Xu, D.P. Sutherland, T.R. Kollmann, M. Liu, S.E. Turvey, Amino acid-dependent attenuation of toll-like receptor signaling by peptide-gold nanoparticle hybrids, *ACS Nano* 9 (2015) 6774–6784.
- [23] M. Fukata, M. Arditi, The role of pattern recognition receptors in intestinal inflammation, *Mucosal. Immunol.* 6 (2013) 451–463.
- [24] B. Khor, A. Gardet, R.J. Xavier, Genetics and pathogenesis of inflammatory bowel disease, *Nature* 474 (2011) 307–317.
- [25] J.C. Kagan, T. Su, T. Horng, A. Chow, S. Akira, R. Medzhitov, TRAM couples endocytosis of toll-like receptor 4 to the induction of interferon- $\beta$ , *Nat. Immunol.* 9 (2008) 361–368.
- [26] B.O. de, E. Merck, U.A. Hasan, S. Hubac, B. Benguigui, G. Trinchieri, E.E. Bates, C. Caux, Recognition of double-stranded RNA by human toll-like receptor 3 and downstream receptor signaling requires multimerization and an acidic PH, *J. Biol. Chem.* 280 (2005) 38133–38145.
- [27] M. Rutz, J. Metzger, T. Gellert, P. Luppa, G.B. Lipford, H. Wagner, S. Bauer, Toll-like receptor 9 binds single-stranded CpG-DNA in a sequence- and PH-dependent manner, *Eur. J. Immunol.* 34 (2004) 2541–2550.
- [28] M. Lamphier, W. Zheng, E. Latz, M. Spyyee, H. Hansen, J. Rose, M. Genest, H. Yang, C. Shaffer, Y. Zhao, et al., Novel small molecule inhibitors of TLR7 and TLR9: mechanism of action and efficacy in vivo, *Mol. Pharmacol.* 85 (2014) 429–440.
- [29] A. Geremia, P. Biancheri, P. Allan, G.R. Corazza, S.A. Di, Innate and adaptive immunity in inflammatory bowel disease, *Autoimmun. Rev.* 13 (2014) 3–10.
- [30] E. Cario, Toll-like receptors in inflammatory bowel diseases: a decade later, *Inflamm. Bowel. Dis.* 16 (2010) 1583–1597.
- [31] R.B. Sartor, Mechanisms of disease: pathogenesis of Crohn's disease and ulcerative colitis, *Nat. Clin. Pract. Gastroenterol. Hepatol.* 3 (2006) 390–407.
- [32] C.C. Bain, A.M. Mowat, Macrophages in intestinal homeostasis and inflammation, *Immunol. Rev.* 260 (2014) 102–117.
- [33] A. Savva, T. Roger, Targeting toll-like receptors: promising therapeutic strategies for the management of sepsis-associated pathology and infectious diseases, *Front. Immunol.* 4 (2013) 387.

- [34] N. Matsunaga, N. Tsuchimori, T. Matsumoto, M. Ii, TAK-242 (resatorvid), a small-molecule inhibitor of toll-like receptor (TLR) 4 signaling, binds selectively to TLR4 and interferes with interactions between TLR4 and its adaptor molecules, *Mol. Pharmacol.* 79 (2011) 34–41.
- [35] P. Mistry, M.H. Laird, R.S. Schwarz, S. Greene, T. Dyson, G.A. Snyder, T.S. Xiao, J. Chauhan, S. Fletcher, V.Y. Toshchakov, et al., Inhibition of TLR2 signaling by small molecule inhibitors targeting a pocket within the TLR2 TIR domain, *Proc. Natl. Acad. Sci. U. S. A.* 112 (2015) 5455–5460.
- [36] L. Foit, C.S. Thaxton, Synthetic high-density lipoprotein-like nanoparticles potentially inhibit cell signaling and production of inflammatory mediators induced by lipopolysaccharide binding toll-like receptor 4, *Biomaterials* 100 (2016) 67–75.
- [37] C.Y. Tsai, S.L. Lu, C.W. Hu, C.S. Yeh, G.B. Lee, H.Y. Lei, Size-dependent attenuation of TLR9 signaling by gold nanoparticles in macrophages, *J. Immunol.* 188 (2012) 68–76.
- [38] V. Deretic, T. Saitoh, S. Akira, Autophagy in infection, inflammation and immunity, *Nat. Rev. Immunol.* 13 (2013) 722–737.
- [39] C.O. Elson, Y. Cong, V.J. McCracken, R.A. Dimmitt, R.G. Lorenz, C.T. Weaver, Experimental models of inflammatory bowel disease reveal innate, adaptive, and regulatory mechanisms of host dialogue with the microbiota, *Immunol. Rev.* 206 (2005) 260–276.
- [40] A. Kaser, S. Zeissig, R.S. Blumberg, Inflammatory bowel disease, *Annu. Rev. Immunol.* 28 (2010) 573–621.
- [41] L. Henckaerts, M. Pierik, M. Joossens, M. Ferrante, P. Rutgeerts, S. Vermeire, Mutations in pattern recognition receptor genes modulate seroreactivity to microbial antigens in patients with inflammatory bowel disease, *Gut* 56 (2007) 1536–1542.
- [42] C. Abraham, R. Medzhitov, Interactions between the host immune system and microbes in inflammatory bowel disease, *Gastroenterology* 140 (2011) 1729–1737.
- [43] T.T. MacDonald, G. Monteleone, Immunity, inflammation, and allergy in the gut, *Science* 307 (2005) 1920–1925.
- [44] R. Atreya, M.F. Neurath, IBD pathogenesis in 2014: molecular pathways controlling barrier function in IBD, *Nat. Rev. Gastroenterol. Hepatol.* 12 (2015) 67–68.
- [45] E. Louis, J. Belaiche, Hydroxychloroquine (plaquenil) for recurrence prevention of Crohn's disease after curative surgery, *Gastroenterol. Clin. Biol.* 19 (1995) 233–234.
- [46] M.K. Goenka, R. Kochhar, B. Tandia, S.K. Mehta, Chloroquine for mild to moderately active ulcerative colitis: comparison with sulfasalazine, *Am. J. Gastroenterol.* 91 (1996) 917–921.
- [47] J.J. Storhoff, R. Elghanian, R.C. Mucic, C.A. Mirkin, R.L. Letsinger, One-pot colorimetric differentiation of polynucleotides with single base imperfections using gold nanoparticle probes, *J. Am. Chem. Soc.* 120 (1998) 1959–1964.
- [48] Y. Dong, J. Yang, H. Liu, T. Wang, S. Tang, J. Zhang, X. Zhang, Site-specific drug-releasing polypeptide nanocarriers based on dual-PH response for enhanced therapeutic efficacy against drug-resistant tumors, *Theranostics* 5 (2015) 890–904.